Check for updates

Water Resources Research

RESEARCH ARTICLE
10.1029/2022WR032988

Direct Pore-Scale Numerical Simulation of Microbially Induced Calcium Carbonate Precipitation

Mohammad Amin Razbani[1], Espen Jettestuen[2], and Anja Røyne[1]

[1]Njord Centre, Department of Physics, University of Oslo, Oslo, Norway, [2]Norwegian Research Centre AS (NORCE), Bergen, Norway

Key Points:

- Up-scaling parameters are introduced that show how main processes compete for controlling microbially induced calcium carbonate precipitation
- Biomass distribution does not change the up-scaling parameters in a reaction-diffusion scheme
- It is found that pH local distribution is significant and up-scaled pH is different from Darcy-scale model's predictions

Correspondence to:

A. Røyne,
anja.royne@fys.uio.no

Citation:

Razbani, M. A., Jettestuen, E., & Røyne, A. (2023). Direct pore-scale numerical simulation of microbially induced calcium carbonate precipitation. *Water Resources Research*, *59*, e2022WR032988. https://doi.org/10.1029/2022WR032988

Received 9 JUN 2022
Accepted 24 DEC 2022

© 2023. The Authors.
This is an open access article under the terms of the Creative Commons Attribution License, which permits use, distribution and reproduction in any medium, provided the original work is properly cited.

Abstract Microbially induced calcium carbonate precipitation (MICP) is a promising method for eco-friendly solutions in geotechincal engineering. MICP involves highly coupled processes in geochemistry and bacterial metabolism that take place in a porous medium. Advancement of these processes drives calcite crystal growth which leads to a decrease in porosity and permeability of the medium. Mathematical models are being developed and used to predict the fate of system at different conditions. Micro-scale and local bio-geochemical evolution and its role on the overall macroscopic fate of MICP needs further investigation. In this work, a pore-scale reactive transport model of MICP for biocementation is developed in a closed system. MICP is simulated in a sample porous geometry in 2D using a native geochemical solver and a lattice Boltzmann solver that handles diffusive transport. We present reactive-transport factors to up-scale pore-scale effects and quantify the efficiency of MICP at different stages of the process. Our results show that pore-scale effects on the average concentration of urea and calcium are not significant after the initial 20% of urea have been consumed. On the other hand, the pH evolution in the system is significantly affected by pore-scale effects. We also explored effects of biomass density and biomass distribution on the reactive transport factors, as well as the effect of the urea to calcium ratio on the resulting crystallization patterns. We found that a higher ratio of rate of ureolysis to rate of precipitation leads to more nucleation sites and more uniform calcite precipitation in the geometry.

1. Introduction

MICP has found many applications in construction materials as an eco-friendly alternative (Røyne et al., 2019; Seifan et al., 2016; Yip et al., 2022). The most commonly used process for MICP is the ureolytic pathway, where alkalophilic bacteria hydrolyze urea in an enzymatic reaction mediated by the enzyme urease. In the majority of MICP studies, the choice of urease producing micro organism is *S. pasteurii* which can produce a large amount of urease. Ureolytic calcium carbonate precipitation occurring in a porous bed of unconsolidated sand can bind the sand grains and form what is called biocement (Whiffin et al., 2007). This method has been investigated extensively and showed promising results in different applications including self-healing systems (Yip et al., 2022), bioremediation (J. Zhang et al., 2022), fracture sealing (Cuthbert et al., 2013), and soil-improvement (Ghasemi & Montoya, 2022). In the first step of biocementation, a calcium source, most commonly $CaCl_2$ mixed with water to form a calcium rich solution (Nassar et al., 2018). In the next step, the calcium rich solution is mixed with urea and urease producing bacteria. Bacteria utilize urea as an energy source and hydrolyze it using an enzyme called urease. As a result, the pH and inorganic carbon content in the solution increases. This makes the solution supersaturated with respect to calcium carbonate, and calcium carbonate crystals precipitate. The set of reactions that describe this process is listed in Table 1.

1.1. Biogeochemical Processes in MICP

It has been shown that the most important parameters for controlling the outcome of a biocementation process are the concentration of calcium in the solution, the concentration of dissolved inorganic carbon, pH, and the density of nucleation sites available for crystallization (Hammes & Verstraete, 2002). The main processes describing biocementation can be classified into three different categories. In the first category, there are hydrodynamics of flow inside the porous media. The second category includes the chemical kinetics of the system, such as the rates of precipitation and urea hydrolysis. Lastly, the microbiological evolution of the system should be described, which can include equations for growth and decay of biomass. Key parts of biocementation will be explained with more details below.

19447973, 2023, 1, Downloaded from https://agupubs.onlinelibrary.wiley.com/doi/10.1029/2022WR032988 by University Of Oslo, Wiley Online Library on [15/02/2024]. See the Terms and Conditions (https://onlinelibrary.wiley.com/terms-and-conditions) on Wiley Online Library for rules of use; OA articles are governed by the applicable Creative Commons License

Table 1
Main Chemical Reactions in Biocementation Process[a]

No.	Reaction	logK (25°C)
1	$H_2CO_3 \leftrightarrow HCO_3^- + H^+$	−6.352
2	$HCO_3^- \leftrightarrow CO_3^{2-} + H^+$	−10.329
3	$H_2O \leftrightarrow H^+ + OH^-$	−14.0
4	$CO(NH_2)_2 + 2H_2O \rightarrow H_2CO_3 + 2NH_3$	
5	$NH_3 + H^+ \leftrightarrow NH_4^+$	9.23
6	$Ca^{2+} + CO_3^{2-} \leftrightarrow CaCO_3 \downarrow$	8.48
7	$CaOH^+ \leftrightarrow Ca^{2+} + OH^-$	−1.0 to −1.6
8	$CaHCO_3^+ \leftrightarrow Ca^{2+} + HCO_3^-$	−1.106

[a]Parkhurst and Appelo (2013).

The rate of precipitation is determined mainly by the degree of supersaturation of calcite, and by microscopic surface processes (Teng et al., 2000). In this work, only supersaturation is considered for describing the rate of crystal growth, while nucleation is only allowed on given surface sites, randomly assigned at the initiation of the simulations. The rate of dissolution or precipitation of calcite, as a function of supersaturation, can be described using the following model from Palandari and Kharaka (2004):

$$R_p = (k_1 + k_2 a_H)(1 - \Omega), \tag{1}$$

$$\Omega = \frac{a_{CO_3^{2-}} \cdot a_{Ca^{2+}}}{K}, \tag{2}$$

where R_p is rate of dissolution or precipitation in mol $m^{-2}s^{-1}$, and $k_{1,2}$ are constants equal to 1.55×10^{-6} mol $m^{-2}s^{-1}$ and 0.501 mol $m^{-2}s^{-1}$, respectively, at 25°C. Ω is the saturation ratio, $a_{CO_3^{2-}}$ and $a_{Ca^{2+}}$ are the activities of CO_3^{2-} and Ca^{2+}, respectively, and K is the equilibrium constant.

Experimental studies of biocementation show that there can be three distinct steps in precipitation (W. Zhang et al., 2018). In the first step, amorphous calcium carbonate is formed. This phase is highly hydrated and unstable and is transformed to crystalline forms within seconds (Naka & Carney, 2007), first to sub-micron crystals of vaterite, which is an unstable polymorph of calcium carbonate. In the final step, small seeds of vaterite crystals dissolve and re-precipitate as calcite or aragonite, the more stable polymorphs of calcium carbonate. The model of precipitation that is used in this work refers to the latest step in precipitation where super-micron calcite crystals grow.

In biocementation, the precipitation of calcium carbonate is triggered by ureolysis (Equation 4 in Table 1) which is an enzymatic reaction. The kinetics of this reaction can be described by the Michaelis-Menten model (Lauchnor et al., 2015):

$$R_u = R_m \frac{C_u}{C_u + K_M}, \tag{3}$$

in which R_u is the cell dependent rate of ureolysis in mol $CFU^{-1}h^{-1}$, R_m is the maximum rate of ureolysis, C_u is the concentration of urea, and K_M is the concentration of urea where the rate of reaction is half of the maximum. The unit used for measuring biomass concentration in Equation 3 and elsewhere in this paper is based on CFU which stands for colony forming unit. It counts every bacterium in our model as 1 CFU. K_M and R_m depend on specific enzyme-substrate system conditions, mainly the type and amount of enzyme, pH, ionic strength, and temperature (Chang & Chang, 2000).

1.2. Modeling Biocementation

The porosity and permeability evolution in biocementation is of prime concern from a design standpoint. It will also influence the potential course of mineralization as it influences both advective and diffusive transport of reactants. It dictates the mechanical properties of the final product and its potential applications. An understanding of this evolution requires that the geochemical evolution of the system in the porous media is resolved. Due to the heterogeneity of porous media, both the distribution of nucleation sites and biomass and micro-scale reactive transport in the system may be important. Experimental toolboxes are available that capture the micro-scale bio-geochemical evolution of MICP (Kim et al., 2020; Shu et al., 2022; Weinhardt et al., 2021; Zehner et al., 2021, 2020). Pore-scale modeling can be used to investigate such an evolution. It has been shown that models of reactive transport phenomena at the pore-scale make it possible to explain processes that are not easily modeled at the Darcy (continuum) scale, such as the interplay of porous media architecture with other physical and chemical processes (Molins, 2015; Putnis, 2015).

A generic reactive-transport model starts by coupling equations of transport and chemical kinetics to predict the spatial and temporal evolution of flow and concentration of different components in a system (Lichtner, 1985). Direct numerical simulations (DNSs) of reactive-transport at the pore-scale have been used extensively for

19447973, 2023, 1, Downloaded from https://agupubs.onlinelibrary.wiley.com/doi/10.1029/2022WR032988 by University Of Oslo, Wiley Online Library on [15/02/2024]. See the Terms and Conditions (https://onlinelibrary.wiley.com/terms-and-conditions) on Wiley Online Library for rules of use; OA articles are governed by the applicable Creative Commons License

studying geochemistry, flow, mineral dissolution and precipitation, biological activity, and their interconnections in porous media (Steefel et al., 2005). The LB method is suitable for studying dissolution and precipitation in pore-scale (Hiorth et al., 2013). Also, reactive transport LB models have been successfully coupled with individual based models representing dynamics of microbial activity (Graf Von Der Schulenburg et al., 2009; Tian & Wang, 2019). In an individual based model, the bacterial population is modeled by attributing growth parameters to individual bacteria.

So far, most numerical models proposed for studying MICP use the Darcy-scale approach (Ebigbo et al., 2012; Fauriel & Laloui, 2012; Hommel et al., 2015; Landa-Marbán et al., 2021; Minto et al., 2019; Tveit & Marbán, 2022). In this approach, a representative elementary volume which is larger than size of a single pore is defined to introduce volume average quantities, such as volumetric porosity, as continuous functions. Several researchers have pointed out limitations of Darcy-scale modeling of MICP. For example, van Wijngaarden et al. (2016) constructed a 1D model for MICP and concluded that more advanced models are needed to take into account pore-scale processes like placement of bacteria and the geometrical evolution of the sample, because averaging these processes into a continuum model poses significant uncertainties. Barkouki et al. (2011) and Martinez et al. (2014) developed a continuum scale reactive-transport model for MICP. They found that the choice of parameters could not lead to a unique solution, and suggested other spatial and temporal variables, such as the distribution of bacteria, should be included.

Pore-scale modeling of MICP has barely been done. Qin et al. (2016) proposed a pore network method for indirect numerical simulations of MICP at the pore-scale. They represented the architecture of the porous media as a network of spherical pores connected with cylindrical throats, and assumed small variations in quantities inside every pore element. They noted that this assumption probably needs to be justified by direct simulations. T. Zhang and Klapper (2014) developed a pore-scale model for a single pore in MICP. Recently, Nishimura and Matsubara (2021) developed a direct pore-scale model for MICP for a single cell with simplified chemistry. There have been other attempts in pore-scale modeling of not just MICP but enzymatically induced calcium carbonate precipitation (von Wolff et al., 2021). Pore-scale reactive transport models coupled with bacterial activity are well established in the field of bioremediation (Tian & Wang, 2019).

In the present study, we develop a pore-scale model of MICP. The DNS of reactive transport is performed using the LB method coupled with a geochemical solver introduced by Hiorth et al. (2013). Bacterial activities are included using an individual based approach. The model is used to build a bottom-up understanding of MICP. This is achieved by developing functional relationships between ureolysis kinetics, mass transport, and mineral precipitation at the micro-scale.

2. Model Development

The biocementation process is dominated by chemical and biological reactions coupled with transport of solutes and the geometrical evolution of the system. The equation of advection-diffusion, which is a conservation equation, can describe such a system:

$$\frac{\partial C_i}{\partial t} + \nabla \cdot \left(C_i \vec{v}\right) = \nabla \cdot (D_i \nabla C_i) + Q_i, \tag{4}$$

in which C_i is concentration of species i, v is the advection velocity, D_i is the diffusion constant, and Q_i is a source term. The advection is important when solutes are injected into a specimen, such as in column experiments with continuous flow (Barkouki et al., 2011; Ebigbo et al., 2012).

In this paper, we model a closed system. In such a system diffusion is the mechanism of transport and the advective part of the flux term is zero. This is relevant for applications with pulsed injections of the calcium rich solution into the specimen, where there is no flow for most of the time when crystallization is taking place (Zehner et al., 2021). We, therefore, set v to zero in Equation 4. In our model, we include Equation 4 for all of the active species listed in Table 1 together with equations for chemical equilibrium, and kinetics of both ureolysis and precipitation, which will be presented later in this paper. The governing equations become a set of non-linear partial differential equations. To solve this set of equations, a reactive-transport model is developed and solved using the LB method.

19447973, 2023, 1, Downloaded from https://agupubs.onlinelibrary.wiley.com/doi/10.1029/2022WR032988 by University Of Oslo, Wiley Online Library on [15/02/2024]. See the Terms and Conditions (https://onlinelibrary.wiley.com/terms-and-conditions) on Wiley Online Library for rules of use; OA articles are governed by the applicable Creative Commons License

2.1. The Lattice Boltzmann Method

The lattice Boltzmann method is a numerical modeling approach based on kinetic theory. The variables used in this method are derived from the velocity distributions in the Boltzmann equation, and the macroscopic variables are found as different moment of these distributions (Krüger et al., 2016). The system's geometry is discretized spatially into square nodes. A distribution function is introduced that gives the density of particles in every node and direction as a function of time. This function formulates the fate of a collision by introducing a collision operator:

$$g_\alpha^i(\mathbf{x}+\mathbf{e}_\alpha\delta t, t+\delta t) - g_\alpha^i(\mathbf{x},t) = \Omega_\alpha^i, \tag{5}$$

where g_α^i is the distribution function, $\mathbf{x}$ is the location of each node, $\mathbf{e}$ is a basis velocity, and Ω_α^i is the collision operator. α and i denote velocity direction and species, respectively. In this work, the LB method is used in a two-dimensional geometry with nine basis velocities, which is a common set up of a lattice (Krüger et al., 2016). The Bhathagar-Gross-Krook operator (Qian et al., 1992) is used as a collision operator. This operator is widely used for advection diffusion problems and predicts the effect of a collision based on the difference between the current distribution and equilibrium distributions. The following equations describe the LB method for modeling the diffusion equation (Equation 4):

$$\Omega_\alpha^i = -\frac{\delta t}{\tau}\left[g_\alpha^i(\mathbf{x},t) - g_\alpha^{i,eq}(\rho)\right] + \Delta\Omega_\alpha^i, \tag{6}$$

$$g_\alpha^{i,eq} = w_\alpha C_i, \tag{7}$$

$$\Delta\Omega_\alpha^i = w_\alpha\left(1+\frac{1}{2\tau}\right)Q_i\delta t, \tag{8}$$

$$C_i = \sum_\alpha g_\alpha^i + \frac{1}{2}Q_i\delta t, \tag{9}$$

where g_α^{eq} is an equilibrium distribution function, τ is the relaxation time, $\Delta\Omega_\alpha^i$ is a lattice source term used to include production and consumption of species in chemical reactions, w_α is the weight constant of the lattice, and δt is the time step. The speed in which the system moves toward equilibrium is adjusted using the relaxation time (τ). Using Chapman-Enskog analysis (Chapman et al., 1990), it has been proved that employing Equation 5 with the aforementioned configuration of the lattice at appropriate scale reproduces the diffusion equation in fluids (Equation 4; Wolf-Gladrow, 1995). In this model, physical parameters are related to the LB parameters as follows:

$$D = \frac{1}{3}\left(\tau - \frac{1}{2}\right)\frac{\delta x^2}{\delta t}, \tag{10}$$

where δx and δt are spatial and temporal resolutions respectively.

At the fluid-mineral interface we use a flux boundary condition. In this context, flux is the diffusive flux (g_i^α in Equation 5). There are different approaches for treating heterogeneous reactions in the LB method. We use a link-based method, where the outgoing flux in a specific direction from a wall node is calculated based on the incoming flux from the neighboring node at the opposite direction, and the rate of reaction on the surface (Hiorth et al., 2013; Verhaeghe et al., 2006).

2.2. Biomass Model

In our model, biomass is modeled as a scalar field on top of the diffusive field. In this approach, biomass is not part of the geometry and does not occupy any space there but interacts with it through ureolysis. This simplification is justified by the fact that biomass nodes account for approximately 1% of total nodes in the bulk. Therefore, the bacteria are not part of the mass balance in the LB part of the model. The biomass field is coupled to the diffusion field to see concentration of chemical components and mineral growth. Biomass is regarded as micro-colonies attached to sand grains. Micro-colonies are contrasted from macro-colonies by their size, where micro-colonies have a threshold radius of 100–200μm (Jeanson et al., 2015). Growth in micro-colonies is similar to planktonic growth, and no pH gradient exists inside the colony. We do not add any viable carbon

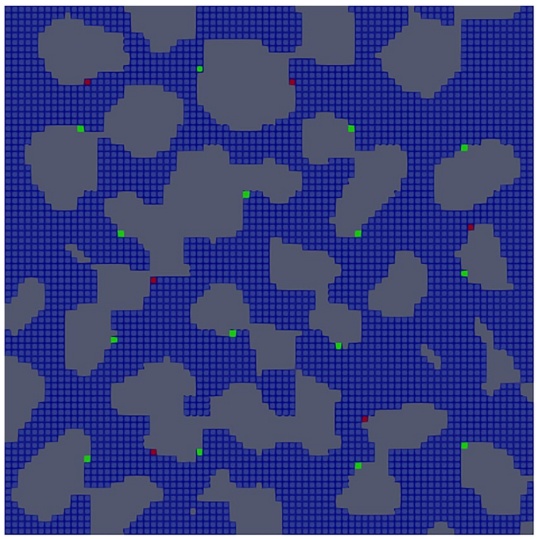

Figure 1. A sample porous geometry (lattice) used in simulating biocementation. Green nodes represent biomass, gray patches are sand grains, and red nodes are nucleation sites.

source or nutrients for the micro-colonies. This is often the case in studies of MICP with a pulsed injection strategy (Lauchnor et al., 2013). Therefore, the micro-colonies do not grow in our simulations, nor do they detach from the surface or break into parts.

Cuthbert et al. (2012) have shown that encapsulation of biomass by calcite crystals limits MICP. In our model, calcite growth in the diffusive field can deactivate biomass wherever they overlap. In this way, the encapsulation and deactivation of bacteria due to calcite growth in MICP can be simulated.

The urease-producing strain used in our model is *S. pasteurii*. The rate of urease production for this strain has been found to be proportional to the biomass concentration (Mobley et al., 1995). Lauchnor et al. (2015) studied MICP using *S. pasteurii* and fit the rate of urea hydrolysis to a Michaelis-Menten relationship for the urea concentration in the range of 1–722 mM. They found the ureolysis rate to be proportional to cell concentration, and reported that NH_4^+, the main product of ureolysis, does not seem to inhibit ureolysis in the range of concentrations relevant for MICP. Considering the findings of Lauchnor et al. (2015) and assuming that only the urea concentration limits ureolysis, we model the kinetics of ureolysis in a biomass node as follows:

$$\frac{dC_u}{dt} = \frac{R_m C_u}{K_M + C_u} C_{sp}, \tag{11}$$

where C_u is the concentration of urea, R_m is the maximum rate constant of ureolysis in a specific biomass concentration and equal to 6.4×10^{-12} mol/CFU/h, K_M is half-saturation constant and equal to 0.305 M, and C_{sp} is the local concentration of *S. pasteurii* bacteria. As we mentioned earlier in this section, in our model the spatial distribution of C_{sp} does not change with time. Although the biomass concentration in a node is constant, biomass nodes can be deactivated due to encapsulation in our model. By doing this, global biomass concentration can change.

2.3. Biomass Density

Experiments have shown that the concentration of *S. pasteurii* in various growth media tends to reach no more than approximately 10^{11} CFU/l (Achal et al., 2009). In the work of Lauchnor et al. (2015), a maximum concentration of $2 \cdot 10^{11}$ CFU/l was reported in their batch experiment with ureolysis. In our model, micro-colonies are placed attached to sand grains. We treat the biomass as unsegregated and unstructured. This means that biomass comprises numerous similar individual agents. The natural disposition of micro-colonies is to fix themselves to a solid surface. Despite this, bacteria can also be found in the bulk in MICP experiments (Lauchnor et al., 2013), but their effect on ureolysis compared to micro-colonies is assumed to be negligible in this work.

S. pasteurii bacteria are rod shaped, approximately 1.3–4.0 μm long and 0.5–1.2 μm in diameter (Bergey & Holt, 1994). We start by a sample porous geometry depicted in Figure 1. Inoculation is done by choosing 15 nodes at the sand surfaces, with the aim of creating the most uniform distribution possible of bacterial micro-colonies. The size of each node is $10^6 \mu m^3$, and we inoculate each node with 400 bacteria. This gives a bulk biomass density of $1.58 \cdot 10^9$CFU/l.

2.4. Lattice Boltzmann Model of MICP

To implement the model introduced in Section 2.2 into the LB solver, we need to evaluate proper source terms from the biomass model and insert them into Equation 6. Because concentration and source terms are coupled, they should be evaluated through solving coupled equations. The following set of equations describe the evolution of urea concentration in LB framework:

$$\frac{dC_u}{dt} = \frac{R_m C_u}{K_M + C_u} C_{sp}, \tag{12}$$

$$\frac{dC_{sp}}{dt} = 0, \tag{13}$$

19447973, 2023, 1, Downloaded from https://agupubs.onlinelibrary.wiley.com/doi/10.1029/2022WR032988 by University Of Oslo, Wiley Online Library on [15/02/2024]. See the Terms and Conditions (https://onlinelibrary.wiley.com/terms-and-conditions) on Wiley Online Library for rules of use; OA articles are governed by the applicable Creative Commons License

19447973, 2023, 1, Downloaded from https://agupubs.onlinelibrary.wiley.com/doi/10.1029/2022WR032988 by University Of Oslo, Wiley Online Library on [15/02/2024]. See the Terms and Conditions (https://onlinelibrary.wiley.com/terms-and-conditions) on Wiley Online Library for rules of use; OA articles are governed by the applicable Creative Commons License

Table 2
Simulation Set-Up and Properties of the Lattice (Geometry)

Parameter	Value
Initial urea concentration	1.0 M
Initial $CaCl_2$ concentration	1.0 M
Size of the lattice	80 × 80nodes
Length resolution	100μm
Initial porosity	0.57

$$C_u = \rho_u + \frac{1}{2}\frac{dC_u}{dt}, \tag{14}$$

$$\rho_u = \sum_{\alpha} g_{\alpha}. \tag{15}$$

Concentration are defined based on definitions provided in Equations 8 and 9. Solving the equations gives us unknown terms, that is, C_u and dC_u/dt:

$$C_u = -\frac{1}{2}K_u + \frac{1}{2}\rho_u + \frac{1}{4}R_m\rho_s \pm \frac{1}{4}\sqrt{\Delta}, \tag{16}$$

$$\Delta \equiv (2K_M - 2\rho_u - R_m\rho_s)^2 + 16\rho_u K_M. \tag{17}$$

It can be shown that there is only one positive solution for C_u, which is achieved by using a positive sign for $\sqrt{\Delta}$ in Equation 16.

2.5. Nucleation Sites

It has been argued that because bacterial surfaces are negatively charged, they may attract calcium cations and serve as nucleation sites for precipitation (Anbu et al., 2016; Hammes & Verstraete, 2002). This argument has been scrutinized in different studies. Microscale experiments have shown that nano-sized calcite crystals form on the surfaces of bacteria during incipient crystallization (Aloisi et al., 2006; Ghosh et al., 2019). On the other hand, W. Zhang et al. (2018) showed by direct measurements that micrometer-sized crystals are not formed on bacteria's surface but further away from them. Bundeleva et al. (2012) suggested the existence of a cell protection mechanism against calcite incrustation. In this work, biomass encapsulation by calcite is not studied. Therefore, nucleation sites are put at least three nodes away from biomass to avoid biomass encapsulation.

The nucleation regime and the prevalence of nucleation sites during precipitation is important in biocementation. The presence of sand grains introduces heterogeneity into the geometry. Interfaces are formed when solid surfaces meet bulk liquid. These interfaces carry a positive free energy that is called surface energy. The energy barrier for nucleation on these surfaces is lower and therefore nucleation on solid-liquid interfaces is thermodynamically favorable (Kelton & Greer, 2010). No new nucleation site emerges during biocementation in this work.

Different regimes of nucleation and crystal growth lead to different evolution of porosity and permeability and this in turn changes mechanical properties of porous geometry (Stack, 2015), but this is not investigated in this work. In this study, nucleation sites are chosen from fluid nodes on the surfaces of sand grains. They are distributed in a way to have the least discrepancy in the distance among them. Therefore we get an almost even nucleation site distribution. Since nucleation sites are active for precipitation since the beginning of any simulation, the whole process is like a seeded crystallization of calcite. The lowest density of nucleation sites was found by considering the results of Lauchnor et al. (2013), which reported that in their experiments with MICP, the saturation index (SI) would reach a maximum of 3.5. We, therefore, chose the lowest number of nucleation sites in our simulation as an input parameter to yield a saturation index of 3.5 locally at maximum.

2.6. Idealized Models

In order to benchmark the LB simulations, two homogeneous (well-mixed) reaction models of MICP, with the same initial condition as those used for the LB model (Table 2), were constructed in the Phreeqc geochemical solver (Parkhurst & Appelo, 2013). In the first model, system is in equilibrium at each step. Precipitation is modeled by removing calcium carbonate from the bulk until saturation is reached and reactants are added incrementally, and the system is in equilibrium at each step. In the second approach, a kinetic model of MICP was constructed inside Phreeqc. In the kinetic model, Equations 1 and 11 were implemented as rate equations. The geochemical solver in the LB simulator has previously been benchmarked against Phreeqc by Hiorth et al. (2010). They showed that the geochemical solver coupled with the LB model can be compared with experimental data.

2.7. Mass Balance

In our closed system, as calcium carbonate precipitates, calcium and carbonate ions are removed from solution so that the total mass of solution decreases. On the other hand, the precipitated calcium carbonate fills some space

19447973, 2023, 1, Downloaded from https://agupubs.onlinelibrary.wiley.com/doi/10.1029/2022WR032988 by University Of Oslo, Wiley Online Library on [15/02/2024]. See the Terms and Conditions (https://onlinelibrary.wiley.com/terms-and-conditions) on Wiley Online Library for rules of use; OA articles are governed by the applicable Creative Commons License

in the pore volume. To track the evolution of the solution volume in a closed system, it is required to calculate the molar volume of aqueous species. The molar volume of ions depends on the ionic strength of the solution and can be calculated using Redlich-type equation (Redlich & Meyer, 1964). Such calculations are not included in the geochemical solver in this work. Periodic boundary conditions are applied at boundaries of the geometry. Therefore, we cannot add and remove fluid from the system without source or sink terms. In this work, the sum of solution volume and volume of precipitated calcite is constant. To check how realistic this assumption is, we calculated the solution volume using Phreeqc which includes proper molar volumes for ions. For the solution described in Table 2, the sum of solution volume and precipitated calcite is not changed til the end when all the initial calcium of 1 M precipitated. Also, the solution volume decreased by 3.7% at the same time.

The change of solution volume changes the concentration of species in the solution. For example, the concentration of inert species should increase a little bit as the pore volume shrinks. In the LB method, this effect is not considered. Physically, It is as if we add some water to the solution and dilute it just enough to compensate for the volume change. Therefore, the concentration of inert species is constant and the effect of change of pore volume on concentrations is ignored. At worst, this will create 3.7% error in the concentrations at the end of each simulation based on the results from Phreeqc. This error is within the uncertainty of the geochemical calculations. These simplifications create a discrepancy in the mass balance over the course of a simulation. The discrepancy in the mass balance is accounted for when simulations are compared with the Phreeqc model. This was done by incorporating the loss of chemical components inside the Phreeqc model based on the data that come from the simulations.

The effect of spatial resolution (δx) was also investigated. The resolution was doubled to see that the LB model can produce consistent results. Comparing concentration of calcium in two different resolutions showed that decreasing the resolution introduces no additional error.

3. Results and Discussions

In the LB model, a 2D geometry represents a biocement specimen. The porous geometry used is depicted in Figure 1. Initial conditions and properties of the system are given in Table 2. The diffusion coefficients for all components in the bulk are considered to be the same and equal to the diffusion coefficient of Ca^{2+} in water. We will see in the next section if this assumption is reasonable. According to Equation 10, the time resolution of our model will be 2.4 s.

3.1. Up-Scaling Pore-Scale Effects

In this section, we up-scale how three main processes in MICP, that is, diffusion, calcite precipitation kinetics and ureolysis kinetics, balance out and control MICP in the whole geometry. To do this, we define two different precipitation factors. The first is the kinetic precipitation factor:

$$\eta_k \equiv \frac{C_{Ca}^{i} - C_{Ca}^{LB}}{C_{Ca}^{i} - C_{Ca}^{k}}, \tag{18}$$

in which i, k, and LB indices refer to the initial condition, the kinetic model, and the LB simulations, respectively. In the idealized system (described in Section 2.6) instead of a porous media, we assume that MICP is happening in a well-mixed bulk. For calculating C_{Ca}^{k}, we include the kinetics of ureolysis and precipitation and only the effect of diffusion is absent. η_k is a function of reaction progress or amount of calcium precipitated and it should be theoretically between zero and one. The closer η_k becomes to one, the more optimized MICP runs in terms of availability of ureolysis products for precipitation. This means higher rate of precipitation relative to the total amount of calcium precipitated. On the other hand, η_k close to zero means that MICP runs with low rate of precipitation, which is not an optimized condition.

To calculate the η_k, the kinetic model presented in Section 2.6 is used to calculate C_{Ca}^{k}. In the kinetic model inside Phreeqc, we start by the same amount of reactive surfaces for nucleation that we have inside LB simulation. In Figure 2, the plot of η_k is presented along with concentrations of calcium and urea in the kinetic model and the LB simulations. Figure 2 also shows that the global urea and calcium concentrations in LB simulation, overlap with their counterparts in the kinetic model. Therefore, the effect of diffusion on these parameters in the

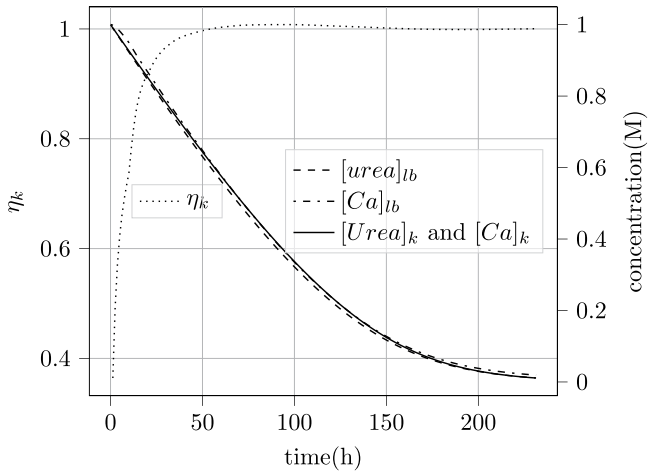

Figure 2. Ureolysis kinetics in an idealized system versus lattice Boltzmann (LB) simulations. Subscripts *lb* and *k* denote LB simulation and the kinetic model respectively. η_k is defined in Equation 18.

pore-scale should be negligible. At the beginning, η_k is close to zero, because right at the beginning there is no precipitation, while ureolysis starts from the first moment. Inspecting reaction rates of ureolysis and precipitation in the Phreeqc model shows that throughout the MICP, reaction rates are equal. Due to slow ureolysis, the same trend is followed in the LB simulations and that is why all concentration profiles almost overlap in Figure 2. We tried two more different initial urea concentration of 0.5 and 2 M. The same trend was observed for rates of precipitation and ureolysis. Therefore we can expect that η_k for different initial concentrations of urea is almost the same.

We call the second type of precipitation factor equilibrium precipitation factor. It quantifies how much calcium is precipitated at each moment in time in the porous media compared to how much would have precipitated if the system was in chemical equilibrium based on the amount of hydrolyzed urea at that moment. The system in chemical equilibrium is the equilibrium model presented in Section 2.6. The equilibrium precipitation factor is defined as follows:

$$\eta_{eq} \equiv \frac{C^i_{Ca} - C^{LB}_{Ca}}{C^i_{Ca} - C^{eq}_{Ca}}, \tag{19}$$

where C^{eq}_{Ca} is the calcium concentration of the equilibrium model. η_{eq} is a measure of how close MICP runs relative to equilibrium. The plot of η_{eq} (Equation 19) is presented in Figure 3. In this figure, one can see that η_{eq} starts off close to zero at the beginning of the MICP and increases sharply to one. As the η_{eq} gets closer to one, the MICP becomes more optimized which means at any urea concentration, a higher amount of calcium is precipitated. As a rule of thumb, in a reaction-diffusion system, as diffusion exerts more control over the whole process (corresponds to high reaction rates), the system distances from equilibrium. On the other hand, if reactions exert more control (corresponding to lower reaction rates), the system gets closer to equilibrium. There are two reaction kinetics in MICP, namely precipitation and ureolysis. Slower ureolysis and faster precipitation gets the system closer to equilibrium. Right at the beginning, the rate of ureolysis is the highest due to higher urea concentration, and the rate of precipitation is the lowest due to lag time it takes for built-up of carbon in the geometry. At the beginning, saturation ratio around nucleation sites is one. As the time goes by, rate of ureolysis decrease and rate of precipitation increases. This means that the system gets closer to equilibrium. From Figure 3, we can say that except the first approximately 20% of the process both in terms of time and urea consumption, the average concentration of calcium in the porous geometry follows the equilibrium model.

More nucleation sites means more reactive surfaces for precipitation, which increases the overall rate of precipitation. Therefore, the ureolysis becomes dominant even sooner in the course of MICP. This means in Figures 2 and 3 the plot of both precipitation factors get closer to one. Since we are already close to equilibrium, higher nucleation densities are not studied. Calcite precipitated at the end of a simulation is shown in Figure 4.

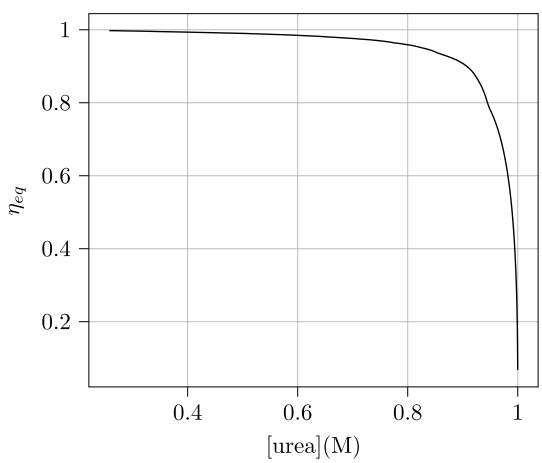

Figure 3. Equilibrium precipitation factor based on Equation 19.

In a non-advective system that we studied, the pore-scale effects are minimized as the reactions get close to equilibrium. In an advective system, pore-scale effects will be pronounced better since fresh reactants are supplied constantly. In such a system, the effect of bacteria transport and attachment would be important. If we lose biomass due to death or encapsulation by calcite, ureolysis rate will get slower and this will shift MICP toward equilibrium even closer. On the other hand, biomass growth in case of supplying nutrients will increase the rate of ureolysis and then we might need to add more nucleation sites. This will need a nucleation criterion to adaptively add nucleation sites in the geometry.

The proposed model and parameters could be used to study other biogeochemical systems involving microbially induced mineral precipitation. Microbially induced carbonates precipitation is used with different microbial

19447973, 2023, 1, Downloaded from https://agupubs.onlinelibrary.wiley.com/doi/10.1029/2022WR032988 by University Of Oslo, Wiley Online Library on [15/02/2024]. See the Terms and Conditions (https://onlinelibrary.wiley.com/terms-and-conditions) on Wiley Online Library for rules of use; OA articles are governed by the applicable Creative Commons License

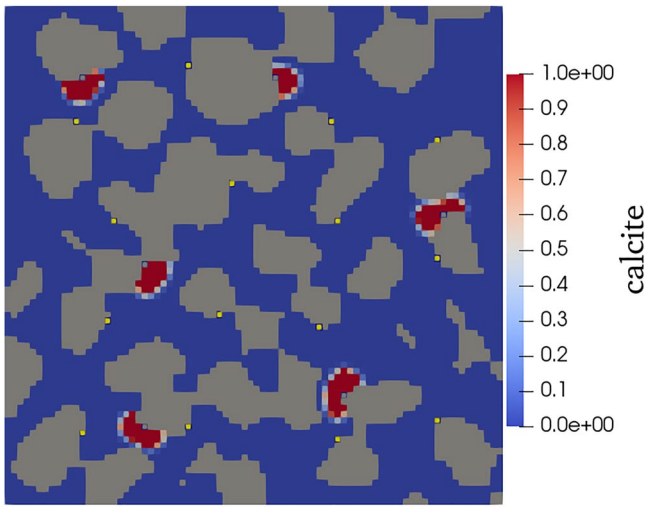

Figure 4. Precipitated calcite at the end of a simulation. Yellow nodes represent biomass, gray patches are sand grains, and gray nodes with edges in the middle of calcite patches are nucleation sites.

groups in addition to ureolytic bacteria for bioremediation of heavy metals from soil through metal carbonate precipitation. Cyanobacteria and algae, nitrate-reducing bacteria, sulfate reducing, ammoniators, and methane oxidants have been used for microbially induced carbonates precipitation (Tamayo-Figueroa et al., 2019).

3.2. Effect of Biomass Distribution and Biomass Density

The effect of biomass distribution on the kinetic and equilibrium precipitation factors was investigated by making different biomass distributions for a single biomass density. Two extra distributions were made by having 30 and 60 biomass nodes in the geometry. These distributions are depicted in Figure 5. Calculating η_{id} and η_{eq} for different biomass distributions showed a negligible deviation of not more than 0.05 between them. It can be concluded that bioamass distribution in the range tested in this work has no effect on η_{id} and η_{eq}. This should be because of the slow rate of ureolysis that gives diffusion enough time to normalize the effect of biomass distribution.

The effect of biomass density on η_{id} and η_{eq} was also tested by decreasing biomass density by two and 10 times of the original biomass density calculated in Section 2.3. Results are shown in Figures 6 and 7. These plots show that decreasing the biomass density shifts η_{id} and η_{eq} toward one, which means that precipitation becomes more efficient. At the same time by decreasing the biomass density, the total time of process increases proportionally. This effect is expected due to the reactive transport nature of MICP described in previous section. By decreasing the biomass density, the system gets closer to the idealized and equilibrium system, introduced in the previous section, because there is more time for the homogenization of the bulk by diffusion.

3.3. Effect of the Initial Conditions

In the last section, we showed that the rate of ureolysis controls the MICP. This rate is the most sensitive to the initial urea concentration according to Equation 11. By increasing the initial urea concentration, the saturation ratio built-up of calcite in the solution is accelerated. There is a maximum saturation ratio before more nucleation sites appear. Saturation ratio cannot increase beyond that maximum because it is thermodynamically unfavorable. Therefore, at higher urea concentrations, more nucleation sites need to be put into the geometry in order to offset the rise of saturation ratio. In this work nucleation sites are always put couple of nodes away from biomass

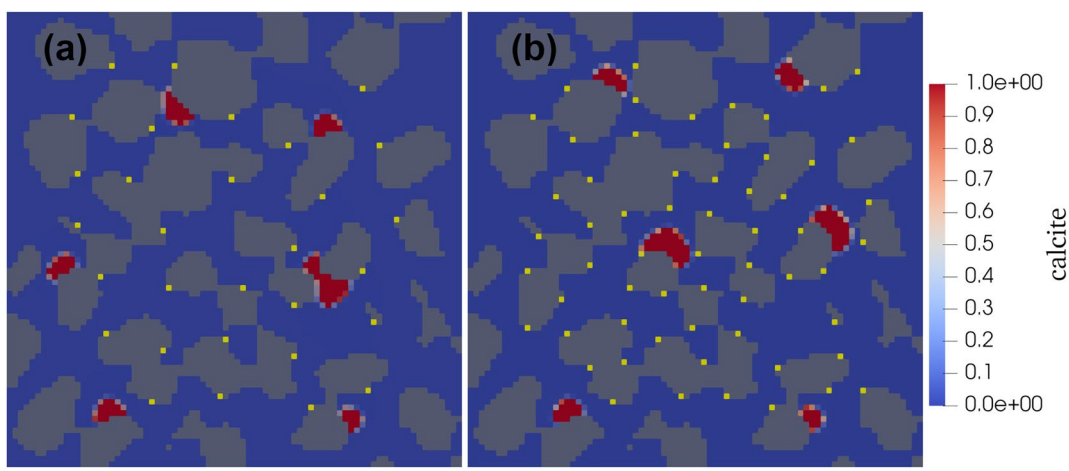

Figure 5. Two different biomass distributions used in simulations of microbially induced calcium carbonate precipitation. Yellow nodes are biomass, red are calcite, gray patches are sand grains and blue shows pore space. The geometry labeled "(a)" has 30 nodes and the one labeled "(b)" has 61 nodes of biomass.

19447973, 2023, 1, Downloaded from https://agupubs.onlinelibrary.wiley.com/doi/10.1029/2022WR032988 by University Of Oslo, Wiley Online Library on [15/02/2024]. See the Terms and Conditions (https://onlinelibrary.wiley.com/terms-and-conditions) on Wiley Online Library for rules of use; OA articles are governed by the applicable Creative Commons License

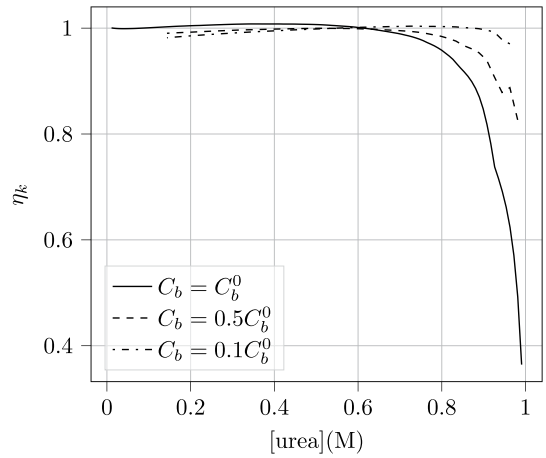

Figure 6. Effect of biomass density (C_b) on η_k (defined in Equation 18), where $C_b^0 = 1.58 \cdot 10^9$ CFU/l.

nodes. Regarding the contrasting findings that were reviewed in Section 2.5, one can assume that a nucleation site happens to be in the same node with a micro-colony in our geometry. In such a case, new rules can be defined in the LB code to handle this situation for deactivating the biomass at appropriate time. By tuning the urea concentration, one can change the number of nucleation sites and this would change the ultimate mechanical properties of MICP. To illustrate this, two extra urea initial conditions are examined in new simulations, at the same conditions mentioned in Table 2 but with urea concentrations of 2 and 0.5 M. For the case of 2 M urea initial concentration, we need to add more nucleation sites to be in the same range of maximum saturation index of 3.5 (like the previous simulations). On the other hand, for the case of 0.5 M initial urea concentration, we need to decrease the number of nucleation sites comparing to the original choice for urea initial concentration of 1 M.

Figure 8 shows when maximum calcium is precipitated at different initial urea concentrations. We can see more nucleation sites at higher urea concentration and vice versa. We do not see any significant change in effectiveness factors with new initial urea concentrations. This is due to the fact that we are in the same range of calcite saturation ratio in all different simulations.

3.4. pH Evolution During MICP

pH is a local parameter in LB simulations. To up-scale pH, we introduce global average pH (pH_{avg}^{LB}) that is calculated from the global arithmetic mean of H^+ concentration. We also introduce $\text{pH}_{\text{min}}^{LB}$ and $\text{pH}_{\text{max}}^{LB}$ in LB simulations as the minimum and maximum pH in the geometry at each step in time. It can be seen from Figure 9 that in the LB simulation pH starts out at a higher value than in the Phreeqc model. The reason is that in LB simulation ureolysis happens instantly from the beginning but precipitation takes time due to transport by diffusion of reactants from biomass sites to nucleation sites. At areas around nucleation sites, precipitation offsets the elevated pH. It is clear from Figure 9 that the effect of pore geometry on pH is significant. In Figure 10, a sample pH distribution in the geometry is presented. It can be seen from the figure that the minimum pH is found around nucleation sites while the maximum pH develops around micro-colonies. The effect of pH on the metabolism of micro-colonies could be important, but it is not investigated in this work. It has been argued that for low Reynolds numbers, biomass creates micro-environments around themselves that leads to a unique precipitation rate (Hammes & Verstraete, 2002). Figure 9 shows that such a local effect can be described well by the LB model.

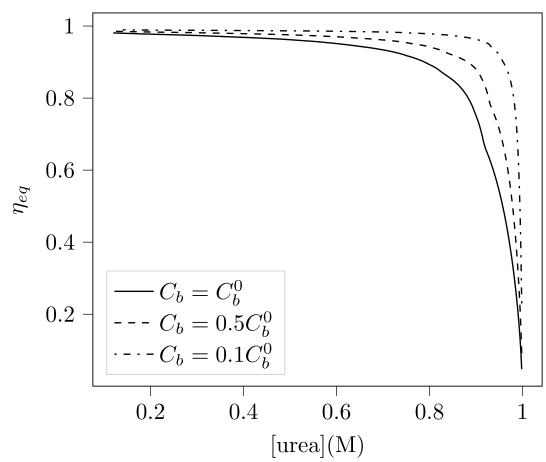

Figure 7. Effect of biomass density (C_b) on η_{eq} (defined in Equation 19), where $C_b^0 = 1.58 \cdot 10^9$ CFU/l.

To find out how sensitive the pH plots are to different choices we made for our case of MICP, different simulations are run. The effect of biomass distribution in terms of number of CFUs in a micro-colony, the number of nucleation sites, and the biomass density as low as one tenth of the original biomass density were tested. Different biomass distribution tested are presented in Figure 5. Results showed that pH development for all simulations are consistent within ±0.1, which is insignificant. Therefore the pH plots presented in Figure 9 should be characteristic of MICP for the case presented in this work and is not sensitive to our choices of biomass density and biomass distribution. This must be because of the fact that rate of ureolysis is not fast enough. Therefore, the biomass density could not change the average pH development. From the other hand, diffusion is fast enough to normalize the effect of biomass distribution. The most important factor here is the initial chemical and geometrical conditions of the system. Changing the initial chemical conditions of the system will change the pH values but not the existence of local pH gradients.

19447973, 2023, 1, Downloaded from https://agupubs.onlinelibrary.wiley.com/doi/10.1029/2022WR032988 by University Of Oslo, Wiley Online Library on [15/02/2024]. See the Terms and Conditions (https://onlinelibrary.wiley.com/terms-and-conditions) on Wiley Online Library for rules of use; OA articles are governed by the applicable Creative Commons License

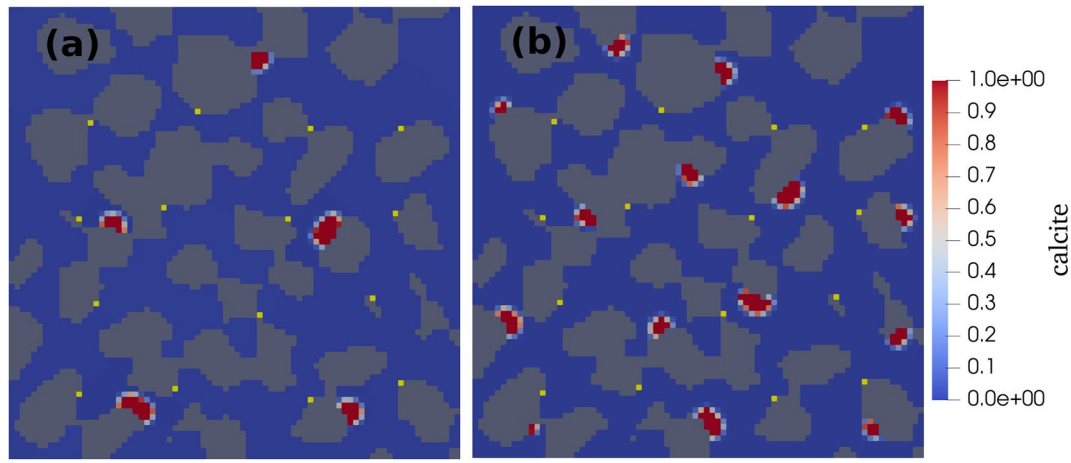

Figure 8. Two different nucleation patterns in simulation of microbially induced calcium carbonate precipitation. Yellow nodes are biomass, red are calcite, gray patches are sand grains and blue shows pore space. The geometry labeled "(a)" starts with 0.5 M urea and the one labeled "(b)" starts with 2 M urea.

4. Conclusion

In this paper, a reactive transport model for biocementation with MICP was developed. A direct numerical simulations of pore-scale MICP was made using the LB method. A simplified model for bacterial ureolysis was implemented that assumes constant ureolysis rate during the course of a simulation.

Two precipitation factors were used to investigate the pore-scale effects. The kinetic precipitation factor showed that except the first 20% of the process, up-scaled kinetics of MICP in our simulations follow the kinetics of an ideal well-mixed system and the process is controlled by the kinetics of ureolysis. Precipitation factors were derived to show how much optimize MICP is running. Equilibrium precipitation factor showed that the system can be considered at equilibrium except for approximately the first 20% of the process.

The biomass distribution was found not to have a significant influence on the precipitation factors. However, the biomass density was found to be important by changing precipitation factors and rate of ureolysis. Significant gradients of local pH were found in the sample, something that is only evident on the pore-scale. Also, the average pH of the system was found to differ from that predicted by the equilibrium model. These observations can be used to improve Darcy-scale models.

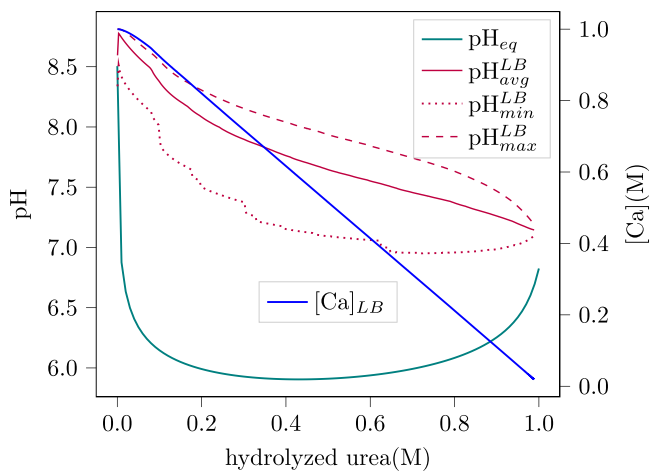

Figure 9. pH evolution of microbially induced calcium carbonate precipitation in lattice Boltzmann simulation in the form of global average (pH^{LB}_{avg}), maximum (pH^{LB}_{max}), and minimum (pH^{LB}_{min}) versus reaction progress. pH_{eq} is the corresponding pH from the equilibrium model and $[Ca]_{LB}$ is the calcium concentration from the LB simulations.

19447973, 2023, 1, Downloaded from https://agupubs.onlinelibrary.wiley.com/doi/10.1029/2022WR032988 by University Of Oslo, Wiley Online Library on [15/02/2024]. See the Terms and Conditions (https://onlinelibrary.wiley.com/terms-and-conditions) on Wiley Online Library for rules of use; OA articles are governed by the applicable Creative Commons License

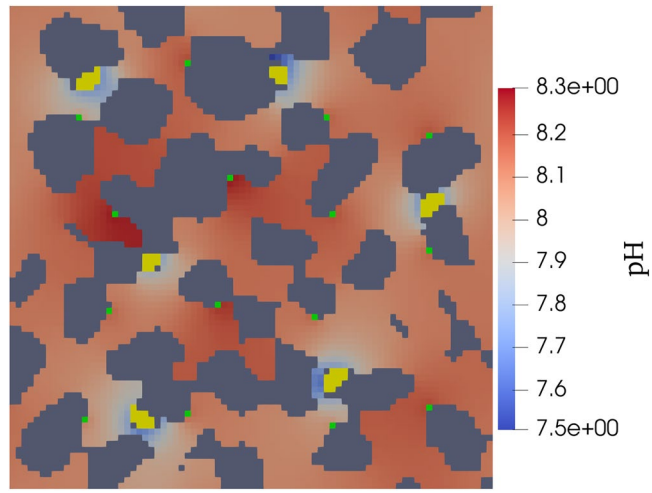

Figure 10. A sample pH distribution during microbially induced calcium carbonate precipitation in lattice Boltzmann simulation. Yellow and green show calcite and biomass, respectively.

While the pore-scale pH evolution in our simulations did not depend on the biomass distribution and biomass density, these factors may be important to include in MICP modeling if the ureolysis kinetics is set to depend on pH. The role of the ratio of urea to calcium initial concentrations on nucleation was explored. With tuning this ratio, one can get different precipitation patterns, considering the properties they expect from the final product. To improve the model presented in this work, a nucleation criterion should be implemented in the model instead of using pre-defined nucleation sites.

Acronyms

MICP	microbially induced calcium carbonate precipitation
LB	lattice Boltzmann
DNS	direct numerical simulation

Data Availability Statement

The code of the LB simulator and a script for Phreeqc simulations can be accessed at Eje74 (2022) and Razbani (2022), respectively.

Acknowledgments
This work was supported by the Research Council of Norway under project 269084/O70.

References

Achal, V., Mukherjee, A., Basu, P. C., & Reddy, M. S. (2009). Strain improvement of *Sporosarcina pasteurii* for enhanced urease and calcite production. *Journal of Industrial Microbiology and Biotechnology*, *36*(7), 981–988. https://doi.org/10.1007/s10295-009-0578-z

Aloisi, G., Gloter, A., Krüger, M., Wallmann, K., Guyot, F., & Zuddas, P. (2006). Nucleation of calcium carbonate on bacterial nanoglobules. *Geology*, *34*(12), 1017–1020. https://doi.org/10.1130/G22986A.1

Anbu, P., Kang, C.-H., Shin, Y.-J., & So, J.-S. (2016). Formations of calcium carbonate minerals by bacteria and its multiple applications. *SpringerPlus*, *5*(1), 250. https://doi.org/10.1186/s40064-016-1869-2

Barkouki, T. H., Martinez, B. C., Mortensen, B. M., Weathers, T. S., De Jong, J. D., Ginn, T. R., et al. (2011). Forward and inverse bio-geochemical modeling of microbially induced calcite precipitation in half-meter column experiments. *Transport in Porous Media*, *90*(1), 23–39. https://doi.org/10.1007/s11242-011-9804-z

Bergey, D., & Holt, J. (1994). *Bergey's manual of determinative bacteriology*. Williams & Wilkins.

Bundeleva, I. A., Shirokova, L. S., Bénézeth, P., Pokrovsky, O. S., Kompantseva, E. I., & Balor, S. (2012). Calcium carbonate precipitation by anoxygenic phototrophic bacteria. *Chemical Geology*, *291*, 116–131. https://doi.org/10.1016/j.chemgeo.2011.10.003

Chang, R., & Chang, R. (2000). *Physical chemistry for the chemical and biological sciences*. University Science Books.

Chapman, S., Cowling, T., Burnett, D., & Cercignani, C. (1990). *The mathematical theory of non-uniform gases: An account of the kinetic theory of viscosity, thermal conduction and diffusion in gases*. Cambridge University Press.

Cuthbert, M. O., McMillan, L. A., Handley-Sidhu, S., Riley, M. S., Tobler, D. J., & Phoenix, V. R. (2013). A field and modeling study of fractured rock permeability reduction using microbially induced calcite precipitation. *Environmental Science & Technology*, *47*(23), 13637–13643. https://doi.org/10.1021/es402601g

Cuthbert, M. O., Riley, M. S., Handley-Sidhu, S., Renshaw, J. C., Tobler, D. J., Phoenix, V. R., & Mackay, R. (2012). Controls on the rate of ureolysis and the morphology of carbonate precipitated by *S. pasteurii* biofilms and limits due to bacterial encapsulation. *Ecological Engineering*, *41*, 32–40. https://doi.org/10.1016/j.ecoleng.2012.01.008

19447973, 2023, 1, Downloaded from https://agupubs.onlinelibrary.wiley.com/doi/10.1029/2022WR032988 by University Of Oslo, Wiley Online Library on [15/02/2024]. See the Terms and Conditions (https://onlinelibrary.wiley.com/terms-and-conditions) on Wiley Online Library for rules of use; OA articles are governed by the applicable Creative Commons License

Ebigbo, A., Phillips, A., Gerlach, R., Helmig, R., Cunningham, A. B., Class, H., & Spangler, L. H. (2012). Darcy-scale modeling of microbially induced carbonate mineral precipitation in sand columns: Modeling MICP in porous media. *Water Resources Research*, *48*(7). https://doi.org/10.1029/2011WR011714

Eje74. (2022). eje74/BioZement: BADChIMP Simulator. *Zenodo*. https://doi.org/10.5281/ZENODO.7462384

Fauriel, S., & Laloui, L. (2012). A bio-chemo-hydro-mechanical model for microbially induced calcite precipitation in soils. *Computers and Geotechnics*, *46*, 104–120. https://doi.org/10.1016/j.compgeo.2012.05.017

Ghasemi, P., & Montoya, B. M. (2022). Field implementation of microbially induced calcium carbonate precipitation for surface erosion reduction of a coastal plain sandy slope. *Journal of Geotechnical and Geoenvironmental Engineering*, *148*(9), 04022071. https://doi.org/10.1061/(ASCE)GT.1943-5606.0002836

Ghosh, T., Bhaduri, S., Montemagno, C., & Kumar, A. (2019). *Sporosarcina pasteurii* can form nanoscale calcium carbonate crystals on cell surface. *PLoS One*, *14*(1), e0210339. https://doi.org/10.1371/journal.pone.0210339

Graf Von Der Schulenburg, D. A., Pintelon, T. R. R., Picioreanu, C., Loosdrecht, M. C. M. V., & Johns, M. L. (2009). Three-dimensional simulations of biofilm growth in porous media. *AIChE Journal*, *55*(2), 494–504. https://doi.org/10.1002/aic.11674

Hammes, F., & Verstraete, W. (2002). Key roles of pH and calcium metabolism in microbial carbonate precipitation. *Reviews in Environmental Science and Biotechnology*, *1*(1), 3–7. https://doi.org/10.1023/A:1015135629155

Hiorth, A., Jettestuen, E., Cathles, L. M., Korsnes, R. I., & Madland, M. V. (2010). A fully coupled geochemical model with a pore-scale lattice Boltzmann simulator - principles and first results.

Hiorth, A., Jettestuen, E., Cathles, L. M., & Madland, M. (2013). Precipitation, dissolution, and ion exchange processes coupled with a lattice Boltzmann advection diffusion solver. *Geochimica et Cosmochimica Acta*, *104*, 99–110. https://doi.org/10.1016/j.gca.2012.11.019

Hommel, J., Lauchnor, E., Phillips, A., Gerlach, R., Cunningham, A. B., Helmig, R., et al. (2015). A revised model for microbially induced calcite precipitation: Improvements and new insights based on recent experiments. *Water Resources Research*, *51*(5), 3695–3715. https://doi.org/10.1002/2014WR016503

Jeanson, S., Floury, J., Gagnaire, V., Lortal, S., & Thierry, A. (2015). Bacterial colonies in solid media and foods: A review on their growth and interactions with the micro-environment. *Frontiers in Microbiology*, *6*. https://doi.org/10.3389/fmicb.2015.01284

Kelton, K. F., & Greer, A. L. (2010). Chapter 6—Heterogeneous nucleation. In K. F. Kelton & A. L. Greer (Eds.), *Pergamon Materials Series* (Vol. 15, pp. 165–226). https://doi.org/10.1016/S1470-1804(09)01506-5

Kim, D., Mahabadi, N., Jang, J., & Paassen, L. A. v. (2020). Assessing the kinetics and pore-scale characteristics of biological calcium carbonate precipitation in porous media using a microfluidic chip experiment. *Water Resources Research*, *56*, e2019WR025420. https://doi.org/10.1029/2019WR025420

Krüger, T., Kusumaatmaja, H., Kuzmin, A., Shardt, O., Goncalo, S., & Viggen, E. M. (2016). *The lattice Boltzmann method: Principles and practice*. Springer Berlin Heidelberg.

Landa-Marbán, D., Tveit, S., Kumar, K., & Gasda, S. E. (2021). Practical approaches to study microbially induced calcite precipitation at the field scale. *International Journal of Greenhouse Gas Control*, *106*, 103256. https://doi.org/10.1016/j.ijggc.2021.103256

Lauchnor, E., Schultz, L. N., Bugni, S., Mitchell, A. C., Cunningham, A. B., & Gerlach, R. (2013). Bacterially induced calcium carbonate precipitation and Strontium coprecipitation in a porous media flow system. *Environmental Science & Technology*, *47*(3), 1557–1564. https://doi.org/10.1021/es304240y

Lauchnor, E., Topp, D., Parker, A., & Gerlach, R. (2015). Whole cell kinetics of ureolysis by *Sporosarcina pasteurii*. *Journal of Applied Microbiology*, *118*(6), 1321–1332. https://doi.org/10.1111/jam.12804

Lichtner, P. C. (1985). Continuum model for simultaneous chemical reactions and mass transport in hydrothermal systems. *Geochimica et Cosmochimica Acta*, *49*(3), 779–800. https://doi.org/10.1016/0016-7037(85)90172-3

Martinez, B., De Jong, J., & Ginn, T. (2014). Bio-geochemical reactive transport modeling of microbial induced calcite precipitation to predict the treatment of sand in one-dimensional flow. *Computers and Geotechnics*, *58*, 1–13. https://doi.org/10.1016/j.compgeo.2014.01.013

Minto, J. M., Lunn, R. J., & El Mountassir, G. (2019). Development of a reactive transport model for field-scale simulation of microbially induced carbonate precipitation. *Water Resources Research*, *55*, 7229–7245. https://doi.org/10.1029/2019WR025153

Mobley, H. L., Island, M. D., & Hausinger, R. P. (1995). Molecular biology of microbial ureases. *Microbiological Reviews*, *59*(3), 451–480. https://doi.org/10.1128/mr.59.3.451-480.1995

Molins, S. (2015). Reactive interfaces in direct numerical simulation of pore-scale processes. *Reviews in Mineralogy and Geochemistry*, *80*(1), 461–481. https://doi.org/10.2138/rmg.2015.80.14

Naka, K., & Carney, C. K. (Eds.). (2007). *Biomineralization. 1: Crystallization and self-organization process* (Vol. 270). Springer. (OCLC: 180031509).

Nassar, M. K., Gurung, D., Bastani, M., Ginn, T. R., Shafei, B., Gomez, M. G., et al. (2018). Large-scale experiments in microbially induced calcite precipitation (MICP): Reactive transport model development and prediction. *Water Resources Research*, *54*(1), 480–500. https://doi.org/10.1002/2017WR021488

Nishimura, I., & Matsubara, H. (2021). Coupling simulation of microbially induced carbonate precipitation and bacterial growth using reaction-diffusion and homogenization systems. *Acta Geotechnica*, *16*(5), 1315–1330. https://doi.org/10.1007/s11440-021-01178-w

Palandari, J. L., & Kharaka, Y. K. (2004). A compilation of rate parameters of water-mineral interaction kinetics for application to geochemical modeling (Open-File Report). *U.S. Geological Survey*.

Parkhurst, D. L., & Appelo, C. (2013). *Description of input and examples for Phreeqc version 3: A computer program for speciation, batch-reaction, one-dimensional transport, and inverse geochemical calculations (USGS numbered series No. 6-A43)*. U.S. Geological Survey. https://doi.org/10.3133/tm6A43

Putnis, A. (2015). Transient porosity resulting from fluid-mineral interaction and its consequences. *Reviews in Mineralogy and Geochemistry*, *80*(1), 1–23. https://doi.org/10.2138/rmg.2015.80.01

Qian, Y. H., D'Humières, D., & Lallemand, P. (1992). Lattice BGK models for Navier-Stokes equation. *Europhysics Letters*, *17*(6), 479–484. https://doi.org/10.1209/0295-5075/17/6/001

Qin, C.-Z., Hassanizadeh, S. M., & Ebigbo, A. (2016). Pore-scale network modeling of microbially induced calcium carbonate precipitation: Insight into scale dependence of biogeochemical reaction rates. *Water Resources Research*, *52*(11), 8794–8810. https://doi.org/10.1002/2016WR019128

Razbani, A. (2022). aminraz/Phreeqc: MICP Kinetics. *Zenodo*. https://doi.org/10.5281/ZENODO.7447278

Redlich, O., & Meyer, D. M. (1964). The molal volumes of electrolytes. *Chemical Reviews*, *64*(3), 221–227. https://doi.org/10.1021/cr60229a001

Røyne, A., Phua, Y. J., Balzer Le, S., Eikjeland, I. G., Josefsen, K. D., Markussen, S., et al. (2019). Towards a low CO_2 emission building material employing bacterial metabolism (1/2): The bacterial system and prototype production. *PLoS One*, *14*(4), e0212990. https://doi.org/10.1371/journal.pone.0212990

19447973, 2023, 1, Downloaded from https://agupubs.onlinelibrary.wiley.com/doi/10.1029/2022WR032988 by University Of Oslo, Wiley Online Library on [15/02/2024]. See the Terms and Conditions (https://onlinelibrary.wiley.com/terms-and-conditions) on Wiley Online Library for rules of use; OA articles are governed by the applicable Creative Commons License

Seifan, M., Samani, A. K., & Berenjian, A. (2016). Bioconcrete: Next generation of self-healing concrete. *Applied Microbiology and Biotechnology*, *100*(6), 2591–2602. https://doi.org/10.1007/s00253-016-7316-z

Shu, S., Chen, H., & Meng, H. (2022). Modeling microbially induced carbonate precipitation (MICP) in microfluidic porous chips. *Geofluids*, *2022*, e3616473. https://doi.org/10.1155/2022/3616473

Stack, A. G. (2015). Precipitation in pores: A geochemical Frontier. *Reviews in Mineralogy and Geochemistry*, *80*(1), 165–190. https://doi.org/10.2138/rmg.2015.80.05

Steefel, C., Depaolo, D., & Lichtner, P. (2005). Reactive transport modeling: An essential tool and a new research approach for the Earth sciences. *Earth and Planetary Science Letters*, *240*(3–4), 539–558. https://doi.org/10.1016/j.epsl.2005.09.017

Tamayo-Figueroa, D. P., Castillo, E., & Brandão, P. F. B. (2019). Metal and metalloid immobilization by microbiologically induced carbonates precipitation. *World Journal of Microbiology and Biotechnology*, *35*(4), 58. https://doi.org/10.1007/s11274-019-2626-9

Teng, H. H., Dove, P. M., & De Yoreo, J. J. (2000). Kinetics of calcite growth: Surface processes and relationships to macroscopic rate laws. *Geochimica et Cosmochimica Acta*, *64*(13), 2255–2266. https://doi.org/10.1016/S0016-7037(00)00341-0

Tian, Z., & Wang, J. (2019). Lattice Boltzmann simulation of biofilm clogging and chemical oxygen demand removal in porous media. *AIChE Journal*, *65*(9), e16661. https://doi.org/10.1002/aic.16661

Tveit, S., & Marbán, D. L. (2022). Field-scale optimization of injection strategies for leakage mitigation using microbially induced calcite precipitation. https://doi.org/10.13140/RG.2.2.22042.16324

van Wijngaarden, W. K., van Paassen, L. A., Vermolen, F. J., van Meurs, G. A. M., & Vuik, C. (2016). A reactive transport model for biogrout compared to experimental data. *Transport in Porous Media*, *111*(3), 627–648. https://doi.org/10.1007/s11242-015-0615-5

Verhaeghe, F., Arnout, S., Blanpain, B., & Wollants, P. (2006). Lattice-Boltzmann modeling of dissolution phenomena. *Physical Review E*, *73*(3), 036316. https://doi.org/10.1103/PhysRevE.73.036316

von Wolff, L., Weinhardt, F., Class, H., Hommel, J., & Rohde, C. (2021). Investigation of crystal growth in enzymatically induced calcite precipitation by micro-fluidic experimental methods and comparison with mathematical modeling. *Transport in Porous Media*, *137*(2), 327–343. https://doi.org/10.1007/s11242-021-01560-y

Weinhardt, F., Class, H., Vahid Dastjerdi, S., Karadimitriou, N., Lee, D., & Steeb, H. (2021). Experimental methods and imaging for enzymatically induced calcite precipitation in a microfluidic cell. *Water Resources Research*, *57*(3), e2020WR029361. https://doi.org/10.1029/2020WR029361

Whiffin, V. S., van Paassen, L. A., & Harkes, M. P. (2007). Microbial carbonate precipitation as a soil improvement technique. *Geomicrobiology Journal*, *24*(5), 417–423. https://doi.org/10.1080/01490450701436505

Wolf-Gladrow, D. (1995). A lattice Boltzmann equation for diffusion. *Journal of Statistical Physic*s, *79*(5–6), 1023–1032. https://doi.org/10.1007/BF02181215

Yip, B., Haniffah, M., Kasiman, E., & Abidin, A. (2022). Research progress on microbial self-healing concrete. *Jurnal Teknologi*, *84*(3), 25–45. https://doi.org/10.11113/jurnalteknologi.v84.17895

Zehner, J., Røyne, A., & Sikorski, P. (2021). A sample cell for the study of enzyme-induced carbonate precipitation at the grain-scale and its implications for biocementation. *Scientific Reports*, *11*(1), 13675. https://doi.org/10.1038/s41598-021-92235-7

Zehner, J., Røyne, A., Wentzel, A., & Sikorski, P. (2020). Microbial-induced calcium carbonate precipitation: An experimental toolbox for in situ and real time investigation of micro-scale pH evolution. *RSC Advances*, *10*(35), 20485–20493. https://doi.org/10.1039/D0RA03897K

Zhang, J., Su, P., & Li, L. (2022). Bioremediation of stainless steel pickling sludge through microbially induced carbonate precipitation. *Chemosphere*, *298*, 134213. https://doi.org/10.1016/j.chemosphere.2022.134213

Zhang, T., & Klapper, I. (2014). Critical occlusion via biofilm induced calcite precipitation in porous media. *New Journal of Physics*, *16*(5), 055009. https://doi.org/10.1088/1367-2630/16/5/055009

Zhang, W., Ju, Y., Zong, Y., Qi, H., & Zhao, K. (2018). In situ real-time study on dynamics of microbially induced calcium carbonate precipitation at a single-cell level. *Environmental Science & Technology*, *52*(16), 9266–9276. https://doi.org/10.1021/acs.est.8b02660

19447973, 2023, 1, Downloaded from https://agupubs.onlinelibrary.wiley.com/doi/10.1029/2022WR032988 by University Of Oslo, Wiley Online Library on [15/02/2024]. See the Terms and Conditions (https://onlinelibrary.wiley.com/terms-and-conditions) on Wiley Online Library for rules of use; OA articles are governed by the applicable Creative Commons License